Effect of driving frequency on electron heating in capacitively coupled RF argon glow discharges at low pressure*

Tagra Samir[1], Yue Liu(刘悦)[1,†], Lu-Lu Zhao(赵璐璐)[1,2], and Yan-Wen Zhou(周艳文)[3]

[1] *Key Laboratory of Materials Modification by Laser, Ion and Electron Beams Ministry of Education, School of Physics, Dalian University of Technology, Dalian* 116024, *China*

[2] *School of Information Science and Engineering, Dalian Polytechnic University, Dalian* 116034, *China*

[3] *School of Materials & Metallurgy, University of Science & Technology Liaoning, Anshan* 114051, *China*

(Received 19 June 2017; revised manuscript received 18 July 2017; published online 30 September 2017)

A one-dimensional (1D) fluid model on capacitively coupled radio frequency (RF) argon glow discharge between parallel-plates electrodes at low pressure is established to test the effect of the driving frequency on electron heating. The model is solved numerically by a finite difference method. The numerical results show that the discharge process may be divided into three stages: the growing rapidly stage, the growing slowly stage, and the steady stage. In the steady stage, the maximal electron density increases as the driving frequency increases. The results show that the discharge region has three parts: the powered electrode sheath region, the bulk plasma region and the grounded electrode sheath region. In the growing rapidly stage (at 18 μs), the results of the cycle-averaged electric field, electron temperature, electron density, and electric potentials for the driving frequencies of 3.39, 6.78, 13.56, and 27.12 MHz are compared, respectively. Furthermore, the results of cycle-averaged electron pressure cooling, electron ohmic heating, electron heating, and electron energy loss for the driving frequencies of 3.39, 6.78, 13.56, and 27.12 MHz are discussed, respectively. It is also found that the effect of the cycle-averaged electron pressure cooling on the electrons is to "cool" the electrons; the effect of the electron ohmic heating on the electrons is always to "heat" the electrons; the effect of the cycle-averaged electron ohmic heating on the electrons is stronger than the effect of the cycle-averaged electron pressure cooling on the electrons in the discharge region except in the regions near the electrodes. Therefore, the effect of the cycle-averaged electron heating on the electrons is to "heat" the electrons in the discharge region except in the regions near the electrodes. However, in the regions near the electrodes, the effect of the cycle-averaged electron heating on the electron is to "cool" the electrons. Finally, the space distributions of the electron pressure cooling the electron ohmic heating and the electron heating at $1/4T$, $2/4T$, $3/4T$, and $4/4T$ in one RF-cycle are presented and compared.

Keywords: capacitively coupled plasmas, electron heating, radio frequency (RF) glow discharges, driving frequency

PACS: 52.25.Jm, 52.30.Ex, 52.80.–s **DOI:** 10.1088/1674-1056/26/11/115201

1. Introduction

Capacitively coupled radio frequency (RF) glow discharge at low pressure can generate low temperature plasmas easily. The plasmas, which usually are called capacitively coupled plasmas or CCPs in short, have been widely used in many fields, such as microelectronics, materials processing, metallurgy, and biology. In order to improve efficiencies of all these applications, it is very important to understand the generating mechanism and physical characteristics of the plasmas.

In the past decades, many research studies of CCPs have been conducted both theoretically and experimentally.[1–10] Makabe *et al.* investigated the structure of RF glow discharge in argon at 13.56 MHz by modeling and diagnostics.[1] Richards *et al.* studied argon RF glow discharges by continuum modeling.[2] Kushner examined the electron properties in parallel plate capacitively coupled RF discharges by Monte–Carlo simulation.[6] Meyyappen and Govindan gave a fluid model for RF discharge simulation.[7] Lymberopoulos and Economou investigated the effect of the metastable atoms on the RF glow discharge in argon by fluid simulation.[8] They also developed a PIC/dynamic MC model to study the spatiotemporal electron dynamics in RF glow discharges.[9]

For CCP from RF glow discharge, the driving frequency is a very important operating parameter. Thus, many research efforts have been devoted to the driving frequency.[11–25] The modeling can be performed by using fluid, kinetic, or hybrid models. Nakano and Makabe investigated the effect of driving frequency on the structure of RF discharge by the relaxation continuum model in a narrow-gap reactive-ion etcher with parallel-plate geometry in SF_6 for driving frequencies ranging from 100 kHz to 13.56 MHz.[15] They found that the electron and ion densities increased as the driving frequency increased, however, the sheath width and ion energy decreased with increasing the driving frequency because of a decrease in the magnitude of the dc bias. Segawa *et al.* analyzed the CCPs between parallel plates in CF_4 as a function of the driving frequency between 13.56 and 200 MHz for 50

*Project supported by the National Natural Science Foundation of China (Grant No. 51172101).

†Corresponding author. E-mail: liuyue@dlut.edu.cn

© 2017 Chinese Physical Society and IOP Publishing Ltd

and 200 mTorr by using a fluid model.[16] They found that the sustaining mechanism and spatiotemporal structure depend on the driving frequency and the mean energy of ions. Also, they found that the degree of electro-negativity strongly depends on the pressure and the electro-negativity becomes weaker at low pressure. Colgan *et al.* used self-consistent fluid equations to study electrical characteristics of argon discharges at frequencies varying between 13.56 and 54.4 MHz.[17] They found that electron density scales with the square of driving frequency at constant pressure and applied voltage. Vahedi *et al.*[18] explained the influences of different frequencies by presenting the two-dimensional (2D) results based on direct implicit PIC/MC simulation for capacitive argon RF discharge, as being due to the fact that as the driving frequency increases, the sheath width decreases, and the bulk plasma becomes more uniform. The effects of single and dual driving frequency on glow discharges were also studied.[22]

In a gas discharge, the electrons obtain energy from the electric field and then they are ionized. Therefore, the electron heating mechanism plays an important role in the process of the gas discharge. The electron heating in low pressure discharge has been investigated by using different models.[21–35] Surendra and Graves used particle-in-cell simulations to study the structure of RF glow discharge in pure helium between parallel plate electrodes as well as the ohmic heating.[21] They found that in the absence of secondary electron emission, electron heating in both the sheath regions of the discharge is enhanced at higher voltages compared with ohmic heating in the bulk of the plasma. Kawamura *et al.* investigated the stochastic heating phenomena in single and dual frequency capacitive discharges.[22] They found that for a uniform fixed-ion discharge, in which the ions are assumed to have a uniform density profile, there is no stochastic heating as expected. Zhu *et al.* experimentally investigated the RF power distribution between the electron heating and the ion acceleration by measuring the electron densities and ion energies for different RF driving frequencies (13.56, 27.12, 60, and 156 MHz). They used an inhomogeneous model accounting for different heating mechanisms to compare with the experimental results.[25] Graves used fluid model simulations of a 13.56 MHz RF discharge to study the time and space dependence of rate of electron impact excitation.[26] He found that the electron heating by the RF field peaks at both the sheath regions boundary, resulting in a local rise in electron mean energy there. Nitschke and Graves studied period-averaged electron heating with PIC model and fluid model. They found a difference below 100 mTorr, i.e., in the period-averaged electron heating, the discharge properties predicted by different models are different. They estimated that the electron power input can be improved in the fluid simulation by including an analytic expression for stochastic heating in the electron energy balance equation.[31] Recently, Liu *et al.* used a fluid model to study the effect of the secondary electron emission on the discharge characteristics in a low pressure capacitive RF argon discharge.[34] They found that when the secondary electron emission coefficient varies from 0.01 to 0.3, the electron net power absorption and the electron heating rate have different degrees of enhancement and the electron heating mainly takes place in both sheath regions. Lafleur *et al.* revisited the problem of electron heating in CCPs, and they proposed a method of quantifying the levels of collisionless and collisional heating in plasma.[35]

The effect of the driving frequency on the electron heating in capacitive RF glow discharge at low pressure is a very important physical problem but it is still not clear. In this work, we focus on this effect by means of a numerical simulation. For this aim, a fluid model of the CCPs is established and numerically solved to obtain the numerical results for the driving frequencies of 3.39, 6.78, 13.56 and 27.12 MHz. Analyzing these results, we can draw some conclusions. This paper presents a foundational study on CCPs. The rest of this paper is organized as below. In Section 2, we establish a model. In Section 3 we discuss the results of argon glow discharges for the cases of four different frequencies. Finally, we draw some conclusions from the present study in Section 4.

2. Model

Considering an RF low pressure glow discharge between two parallel-plates. When the electric potential difference between the electrodes reaches a certain value, the gas discharge will take place between the electrodes, thus generating a plasma. The plasma can be described by using a fluid model. Although the sizes of the electrodes are much larger than the gap between the electrodes, a one-dimensional (1D) model can be used.

In the plasma generated in the capacitively coupled RF argon glow discharge at low pressure, the particle species are electron (e), argon atom (Ar), and argon ion (Ar^+), and among them takes place the following reaction: $e + Ar \rightarrow Ar^+ + 2e$. Thus, the density of the ions satisfies[8,34]

$$\frac{\partial n_i}{\partial t} + \frac{\partial J_i}{\partial x} = S; \tag{1}$$

the density of the electrons satisfies

$$\frac{\partial n_e}{\partial t} + \frac{\partial J_e}{\partial x} = S. \tag{2}$$

The ion flux and electron flux in the drift-diffusion approximation are expressed as

$$J_i = -D_i \frac{\partial n_i}{\partial x} + \mu_i n_i E, \tag{3}$$

$$J_e = -D_e \frac{\partial n_e}{\partial x} - \mu_e n_e E, \tag{4}$$

where D_i and D_e are the ion and electron diffusion coefficient, respectively; μ_i and μ_e are the ion and electron mobility, respectively. The source term can be read as

$$S = k_I n_n n_e, \tag{5}$$

where n_n is the density of neutral atoms of the gas. It can be written as $n_n = 3.22 \times 10^{16}\ p\ (\mathrm{cm}^{-3})$, with p being the pressure of the neutral gas. Equation (5) means that in the source term, only the is considered. For the argon discharge, the ionization rate can be written as

$$k_I = k_{I0} \exp\left(-E_I/T_e\right), \tag{6}$$

where T_e is the electron temperature in units of eV. The electron energy balance is evaluated from

$$\frac{\partial}{\partial t}\left(\frac{3}{2} n_e k T_e\right) = -\frac{\partial q_e}{\partial x} + P_c - P_l, \tag{7}$$

$$q_e = -K_e \frac{\partial T_e}{\partial x} + \frac{5}{2} k T_e J_e, \tag{8}$$

$$K_e = \frac{3}{2} k D_e n_e, \tag{9}$$

$$P_c = -e J_e E, \tag{10}$$

$$P_l = H_I S, \tag{11}$$

where q_e is the conductive heat flux of electron energy, K_e is the thermal conductive coefficient, P_c is the electron heating coming from the electron current coupled with the electric field as seen in Eq. (10), and P_l describes the electron energy loss due to the ionization as seen in Eq. (11). For the electron heating coming from the electron current, it has two parts, i.e., the electron cooling coming from the electron pressure and the electron heating coming from the ohmic heating. That is,

$$P_c = P_p + P_h, \tag{12}$$

where

$$P_p = e D_e \frac{\partial n_e}{\partial x} E, \tag{13}$$

$$P_h = e \mu_e n_e E^2. \tag{14}$$

In this work, P_p is called the electron pressure cooling, P_h the electron ohmic heating, and P_c the electron heating. The electric field satisfies

$$-\frac{\partial^2 V}{\partial x^2} = \frac{e}{\varepsilon_0}\left(n_i - n_e\right), \tag{15}$$

$$E = -\frac{\partial V}{\partial x}, \tag{16}$$

where e is the elementary charge and ε_0 is the vacuum permittivity of free space.

In this work, the initial conditions are as follows:

$$n_i = n_e = n_\varepsilon \left[\varepsilon + 16\left(1 - \frac{x}{d}\right)^2 \left(\frac{x}{d}\right)^2\right],$$
$$T_e = T_{ei}, \quad V = 0, \quad 0 \le x \le d.$$

The boundary conditions are as follows:
at $x = 0$ (on the powered electrode):[8,34]

$$J_i = \mu_i n_i E, \quad J_e = -k_s n_e - \gamma J_i,$$
$$T_e = T_{eb}, \quad V = V_A \sin(2\pi f t);$$

at $x = d$ (on the grounded electrode): [8,34]

$$J_i = \mu_i n_i E, \quad J_e = k_s n_e - \gamma J_i, \quad T_e = T_{eb}, \quad V = 0,$$

where γ and k_s are the secondary electron emission coefficient and electron recombination coefficient, respectively.

3. Results and discussion

The model mentioned in the above section is numerically solved by a finite difference method. In calculating, the parameter values are shown in Table 1.

To analyze the effect of the driving frequency on the plasma characteristics in the argon glow discharge, the simulations are carried out for the cases of four different frequencies; that is, $f = 3.39$, 6.78, 13.56, and 27.12 MHz.

Table 1. Parameters used in the numerical simulation.

Name	symbol	value	Ref.
Electron diffusivity	$n_n D_e$	$3.86 \times 10^{22}\ \mathrm{cm}^{-1}\cdot\mathrm{s}^{-1}$	[8], [34]
Electron mobility	$n_n \mu_e$	$9.66 \times 10^{21}\ \mathrm{V}^{-1}\cdot\mathrm{cm}^{-1}\cdot\mathrm{s}^{-1}$	[8], [34]
Ion diffusivity	$n_n D_i$	$2.07 \times 10^{18}\ \mathrm{cm}^{-1}\cdot\mathrm{s}^{-1}$	[8], [34]
Ion mobility	$n_n \mu_i$	$4.65 \times 10^{19}\ \mathrm{V}^{-1}\cdot\mathrm{cm}^{-1}\cdot\mathrm{s}^{-1}$	[8], [34]
Electron recombination coefficient	k_s	$1.19 \times 10^{7}\ \mathrm{cm}\cdot\mathrm{s}^{-1}$	[8], [34]
Ionization factor	k_{I0}	$1.235 \times 10^{-7}\ \mathrm{cm}^3\cdot\mathrm{s}^{-1}$	[8], [34]
Activation energy	E_I	18.687 eV	[34]
Electron energy-loss coefficient	H_I	15.7 eV	[8], [34]
Gas pressure	p	1 Torr	
Gap between the electrodes	d	2.5 cm	
Peak RF voltage	V_A	100 V	
Electron temperature at the electrodes	T_{eb}	0.5 eV	
Secondary electron emission	γ	0.01	

Figure 1 shows the time evolutions of the maximal electron densities for the driving frequencies of 3.39, 6.78, 13.56, and 27.12 MHz. The results indicate that the maximal electron densities all increase monotonically as the driving frequency increases. It is found that the evolutions of the maximal electron densities each have three stages. In the first stage, i.e., in a time range from 0 to 20 μs, the electron densities are smaller and increase rapidly. It can be called growing rapidly stage. In the second stage, i.e., in a time range from 20 μs to 120 μs, the electron densities become larger and increase slowly. It can be called growing slowly stage. In the third stage, i.e., after 120 μs, the electron densities reach their steady states and their values are 6.20699×10^{9}, 2.17211×10^{10}, 7.26788×10^{10}, and 2.30745×10^{11} cm^{-3} at the driving frequencies 3.39, 6.78, 13.56, and 27.12 MHz, respectively. It can be called steady stage.

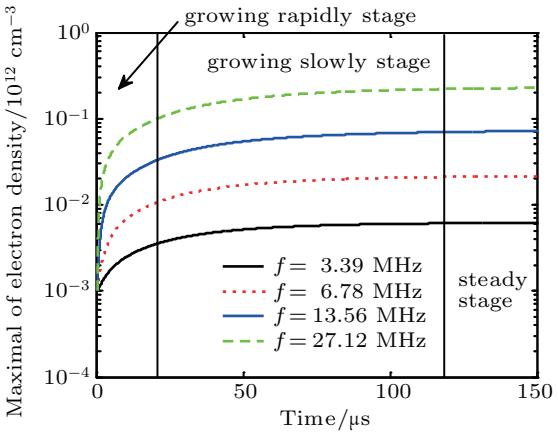


Fig. 1. (color online) Evolutions of the maximal electron densities at driving frequencies of 3.39, 6.78, 13.56, and 27.12 MHz.

Figures 2(a)–2(d) show the cycle-averaged electric fields, electron temperatures, electron densities, and electric potentials are at the steady stage for the driving frequencies of 3.39, 6.78, 13.56, and 27.12 MHz, respectively. The cycle-averaged electric fields between the electrodes at the steady stage are given in Fig. 2(a). The results show that the discharge region has three parts. The first part is the left part of the discharge region and it can be called the powered electrode sheath region. In this region, the electric field is negative. The second part is the right part of the discharge region and it can be called the grounded electrode sheath region. In this region, the electric field is positive. The third part is the middle part of the discharge region and it can be called the bulk plasma region. In this region, the electric field is almost zero (i.e., $\sim$ 0.05 V/cm). In each of the powered electrode sheath region and the grounded electrode sheath region, the width of the sheath decreases as the driving frequency increases and the absolute value of the electric field becomes stronger when the position is close to the electrode. The maximum electric field changes from 153 V/cm at 3.39 MHz to 420 V/cm at 27.12 MHz. The cycle-averaged electron temperatures are plotted in Fig. 2(b). In the bulk plasma region, the electron temperature changes a little, while increasing the driving frequency is almost constant ($\sim$ 1.5 eV). There are two peaks in the powered electrode sheath region and also in the grounded electrode sheath region. The two peaks rise as the driving frequency increases and change from 4.2 eV to 5.3 eV as the driving frequency increases from 3.39 to 27.12 MHz. Also, it is observed the two peaks are closer to the electrodes, respectively. The spatial distributions of the cycle-averaged electron density at the steady stage are presented in Fig. 2(c). The results show that the electron densities increase as the driving frequency increases. In the bulk plasma region, the electron densities grow largely as the driving frequency increases. In the powered electrode sheath region and the grounded electrode sheath region, the electron densities increase slightly with increasing driving frequency. The cycle-averaged electric potentials are shown in Fig. 2(d). In the whole discharge region, it is clear that the potentials increase with increasing driving frequency. In the bulk plasma region, the electric potentials change a little (between 55 V and 60 V) at the driving frequencies of 3.39, 6.78, 13.56, and 27.12 MHz. In the powered electrode sheath region and the grounded electrode sheath region, the electric potentials change from 0 to more than 50 V for all the driving frequencies.

It is most important to study the electron energy transferring mechanism in the rapid growing stage. From Fig. 1, the rapid growing stage is in a time range from 0 to 20 μs. So, we give the cycle-averaged spatial distributions of the electron pressure cooling, the electron ohmic heating, the electron heating and the electron energy loss for driving frequencies of 3.39, 6.78, 13.56, and 27.12 MHz, at 18 μs as shown in Fig. 3. The electron pressure cooling can be calculated from Eq. (13). From Fig. 3(a), it can be seen that in the bulk plasma region, as the driving frequency goes from 3.39 to 27.12 MHz, the electron pressure cooling is almost zero. Also it can be seen that there are two highly negative peaks of the electron pressure cooling in the two sheath regions and these peaks increase negatively as the driving frequency increases. This indicates that the electron pressure cooling mainly occurs in each of the sheath regions. In the powered electrode sheath region the electric field is non-uniform, typically from 0 to negative several hundred V/cm, and the gradient of the electron density is typically highly positive. Therefore, from Eq. (13), in the powered electrode sheath region, the electron pressure cooling is negative. It means that in the powered electrode sheath region, electron pressure cooling cools the electrons. In the grounded electrode sheath region, the electric field is non-uniform, typically from 0 to several hundred V/cm and the gradient of the electron density is typically highly negative. Hence, from Eq. (13), in the grounded electrode sheath region, the electron

pressure cooling is negative. It means that in the grounded electrode sheath region, electron pressure cooling also cools the electrons. These results indicate that the electron pressure cooling takes place mainly in each sheath region and the electron pressure cooling is strongly negative as the driving frequency increases.

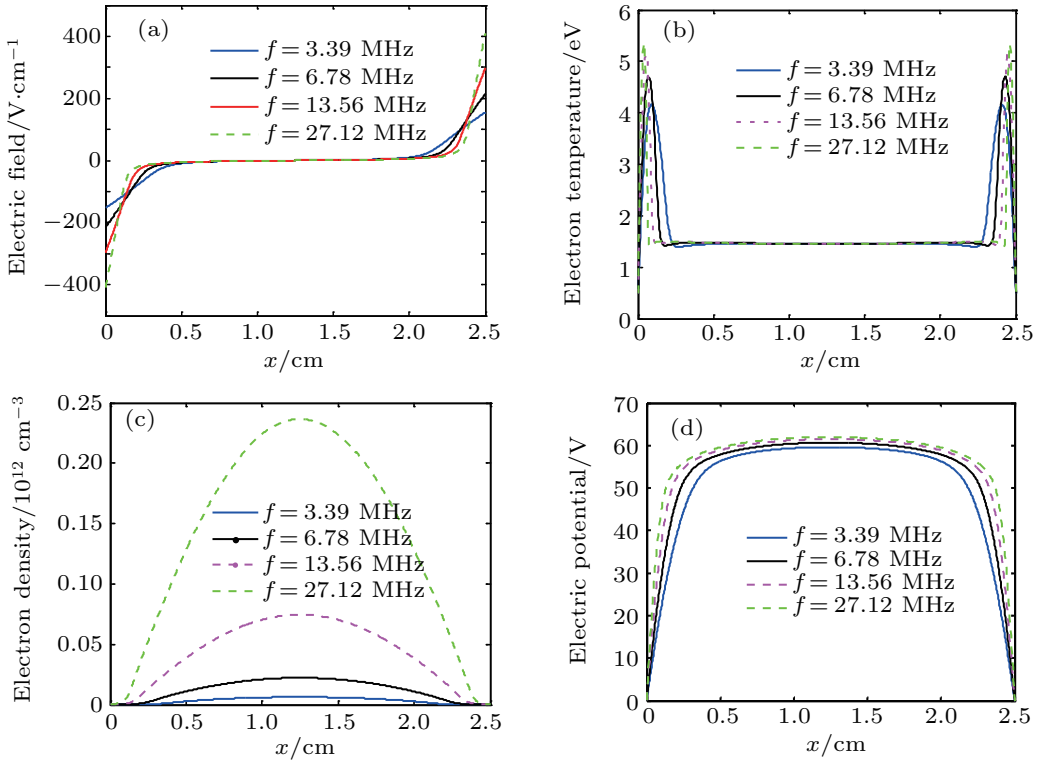


Fig. 2. (color online) Cycle-averaged spatial distributions of (a) electric fields, (b) electron temperatures, (c) electron densities, (d) electric potentials in steady stage at driving frequencies of 3.39, 6.78, 13.56, and 27.12 MHz, respectively.

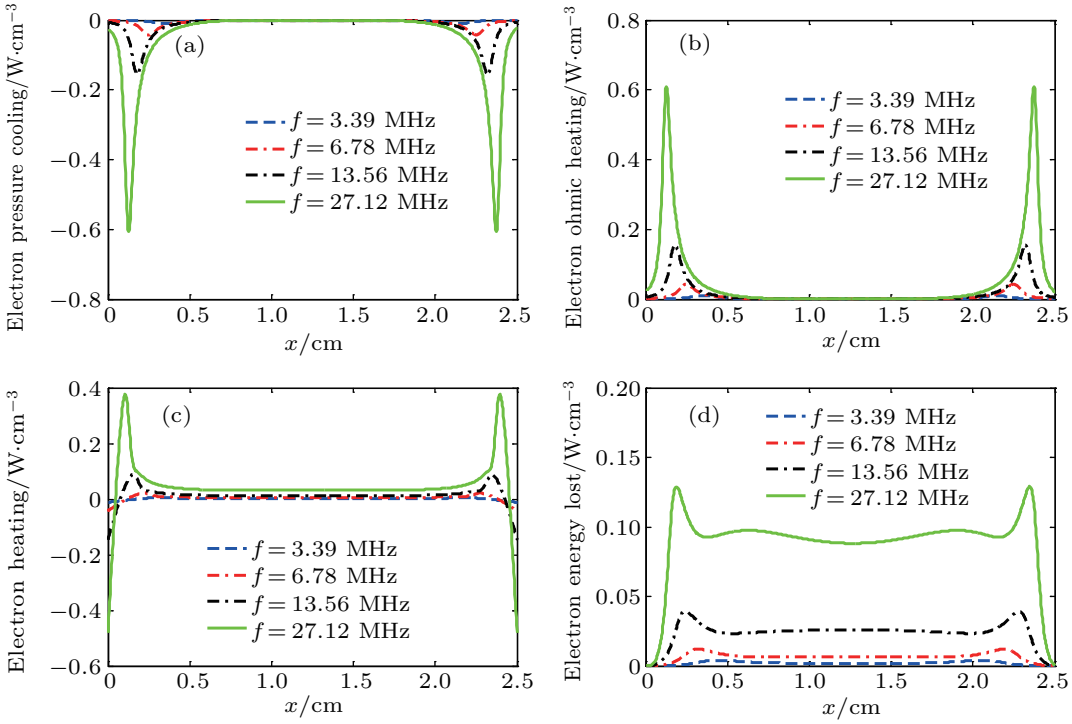


Fig. 3. (color online) Cycle-averaged spatial distributions of (a) electron pressure cooling, (b) electron ohmic heating, (c) electron heating, and (d) electron energy loss at 18 μs for driving frequencies of 3.39, 6.78, 13.56, and 27.12 MHz, respectively.

The electron ohmic heating can be calculated from Eq. (14) and the results are shown in Fig. 3(b). The cycle-averaged electron ohmic heating increases as the driving frequency increases from 3.39 to 27.12 MHz. The results indicate that in the bulk plasma region, the ohmic heating changes from 2.8628×10^{-6} to 0.604681×10^{-3} W·cm^{-3}, which is small, as the driving frequency changes from 3.39 to 27.12 MHz. It is clear that there are two positive peaks of the electron ohmic heating in both sheath regions. In the powered electrode sheath region, the peak increases from 0.10972×10^{-2} W·cm^{-3} at 0.35 cm to 0.603778 W·cm^{-3} at 0.12 cm as the driving frequency increases from 3.39 to 27.12 MHz. In the grounded electrode sheath region, the peak increases from 0.1099×10^{-2} W·cm^{-3} at 2.15 cm to 0.610060 W·cm^{-3} at 2.38 cm as the driving frequency increases from 3.39 to 27.12 MHz. The results indicate that the discharge looks symmetric but it is geometrically asymmetric. The peak values of the electron ohmic heating in the grounded electrode sheath region are greater than those in the powered electrode sheath region. The electron ohmic heating in each of the two sheath regions is large because a large number of electrons are accelerated by the electric fields in the sheath regions compared with in the bulk plasma region.

Figure 3(c) shows the cycle-averaged space distributions of the electron heating, which is composed of the electron pressure cooling and the electron ohmic heating as defined by Eq. (12). The electron heating in the bulk plasma region is positive and increases from 2.195×10^{-3} to 1.276 W/cm^3 as the driving frequency increases from 3.39 to 27.12 MHz. In each of the two sheath regions, the electron heating is positive and increases as the driving frequency increases, except the region near the electrodes where the electron heating takes a negative value. In each of the regions near the electrodes, the electron heating is negative and decreases when the driving frequency increases. The negative electron heating occurs in each of the regions near the electrodes and can be thought of as "diffusion cooling" since electrons diffuse against the local field in each of the regions.

Figure 3(d) shows the variations of cycle-averaged electron energy losses as the driving frequency changes from 3.39 to 27.12 MHz. The cycle-averaged electron energy losses occur in all the discharge regions, and have two peaks in the two sheath regions. As the driving frequency increases, the electron loses its energy rapidly. It is known that the electrons lose their energies as a result of the inelastic collisions between particles and electrons. The electrons gain energies from the electric field and dissipate them by electrons colliding with neutral particles. In particular, the inelastic collisions occur in each sheath region where electron temperature and electric field are large compared with those in the bulk plasma region. The electron energy loss $P_{\rm I} = H_{\rm I}S = H_{\rm I}n_{\rm n}n_{\rm e}k_{\rm I0}\exp(-E_{\rm I}/T_{\rm e})$ depends exponentially on electron temperature but linearly on electron density as given in Eqs. (5), (6), and (11). This dependence is illustrated in Fig. 3(d). It can be seen that in the bulk plasma region, as the driving frequency increases from 3.39 to 27.12 MHz, the electron energy loss increases greatly. Also it can be seen that there are two peaks of the electron energy loss in the two sheath regions and these peaks increase as the driving frequency increases.

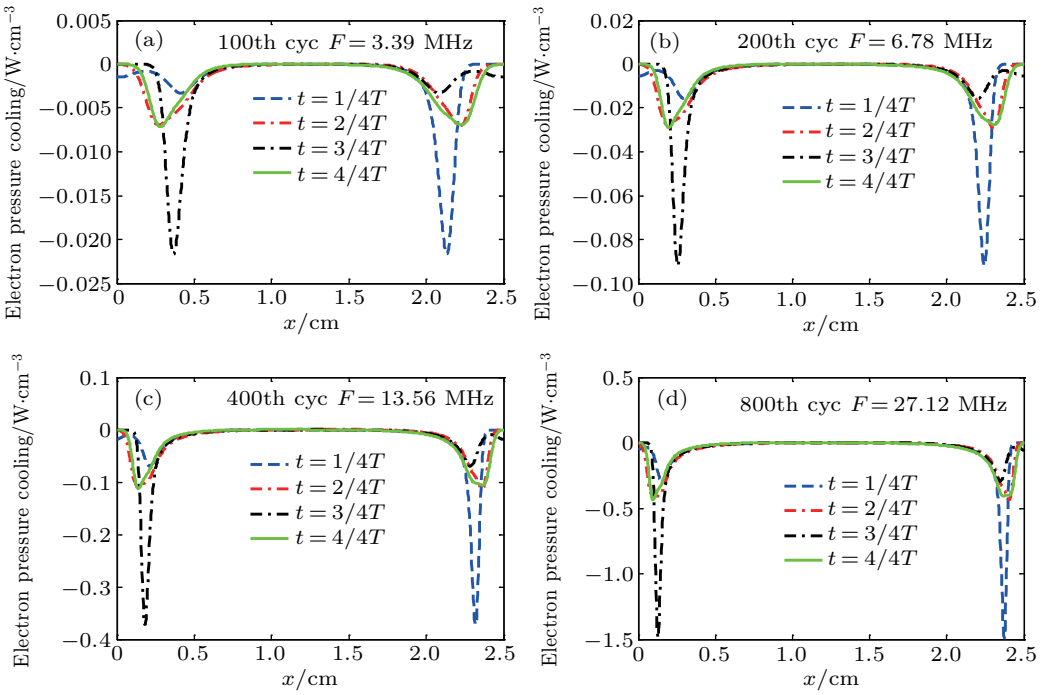


Fig. 4. (color online) Spatial distributions of electron pressure cooling for driving frequencies of (a) 3.39 MHz in the 100th cycle, (b) 6.78 MHz in the 200th cycle, (c) 13.56 MHz in the 400th cycle, and (d) 27.12 MHz in the 800th cycle, at times of $1/4T$, $2/4T$, $3/4T$, and $4/4T$.

The spatial distributions of the electron pressure cooling with the driving frequency 3.39 MHz in the 100th RF cycle, 6.78 MHz in the 200th RF cycle, 13.56 MHz in the 400th RF cycle, and 27.12 MHz in the 800th RF cycle at times $t = 1/4T$, $2/4T$, $3/4T$, and $4/4T$ are plotted in Fig. 4. The results show that at the four times for the four driving frequencies, in the discharge region the electron pressure cooling is negative. This means that the electron pressure cooling always cools the electrons. For the four driving frequencies, at the time $t = 1/4T$, in the powered electrode sheath region, there is a negative peak of the electron pressure cooling; in the grounded electrode sheath region, there is a higher negative peak of the electron pressure cooling; in the bulk plasma region, the electron pressure cooling is negative and almost zero. For the four driving frequencies, at the time $t = 2/4T$, both in the powered electrode sheath region and in the grounded electrode sheath region there is a negative peak of the electron pressure cooling and the two peaks that are mutually the mirror images; in the bulk plasma region, the electron pressure cooling is almost the same one at time $t = 1/4T$. For the four driving frequencies, at time $t = 3/4T$, the electron pressure cooling is just a mirror-imaged one at time $t = 1/4T$. For the four driving frequencies, at time $t = 4/4T$, the electron pressure cooling is almost the same as the one at time $t = 2/4T$. As the driving frequency increases, the electron pressure cooling increases negatively.

The spatial distributions of the electron ohmic heating with the driving frequencies of 3.39 MHz in the 100th RF cycle, 6.78 MHz in the 200th RF cycle, 13.56 MHz in the 400th RF cycle, and 27.12 MHz in the 800th RF cycle at times $t = 1/4T$, $2/4T$, $3/4T$, and $4/4T$ are plotted in Fig. 5. The results show that at the four times for the four driving frequencies, in each case the electron ohmic heating in the discharge region is positive. This means that the electron ohmic heating always heats the electrons. For the four driving frequencies, at the time $t = 1/4T$, in the powered electrode sheath region, there is a peak of the electron ohmic heating; in the grounded electrode sheath region, there is a higher peak of the electron ohmic heating; in the bulk plasma region, the electron ohmic heating is positive and but very small. For the four driving frequencies, at the time $t = 2/4T$, both in the powered electrode sheath region and in the grounded electrode sheath region, there is a peak of the electron ohmic heating and the peak in the powered electrode sheath region is higher than the peak in the grounded electrode sheath region; in the bulk plasma region, the electron ohmic heating is almost the same as one at the time $t = 1/4T$. For the four driving frequencies, at time $t = 3/4T$, the electron ohmic heating is just the mirror-imaged one at time $t = 1/4T$. For the four driving frequencies, at time $t = 4/4T$, the electron ohmic heating is almost the same as one at time $t = 2/4T$. As the driving frequency increases, the electron ohmic heating increases.

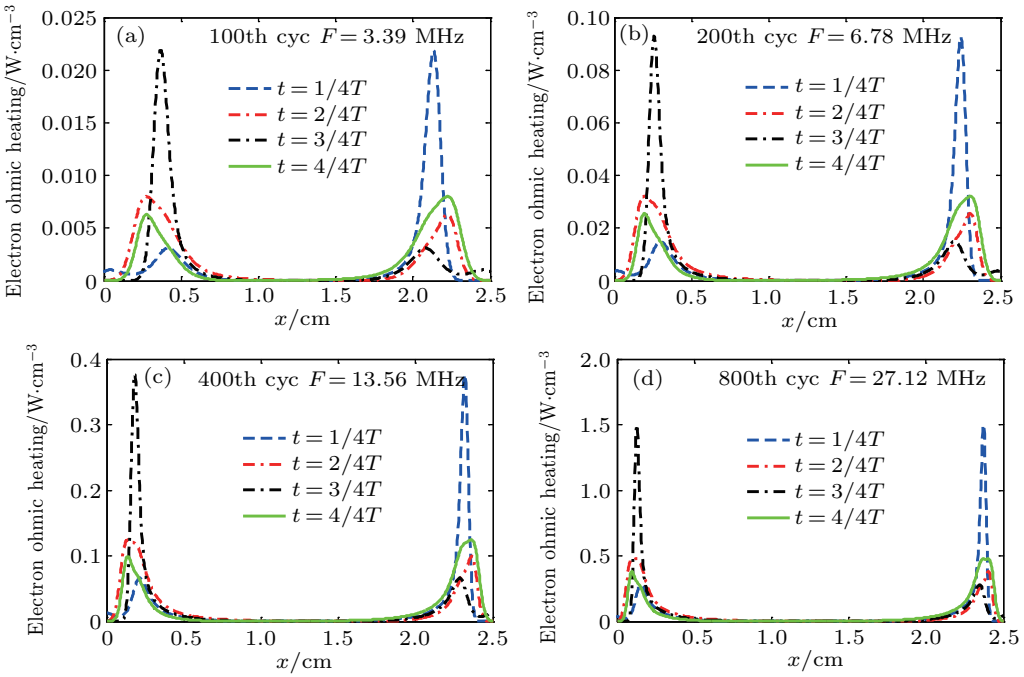


Fig. 5. (color online) Spatial distributions of electron ohmic heating for driving frequencies of (a) 3.39 MHz in the 100th cycle, (b) 6.78 MHz in the 200th cycle, (c) 13.56 MHz in the 400th cycle, and (d) 27.12 MHz in the 800th cycle, at times of $1/4T$, $2/4T$, $3/4T$, and $4/4T$.

The spatial distributions of the electron heating with the driving frequencies of 3.39 MHz in the 100th RF cycle, 6.78 MHz in the 200th RF cycle, 13.56 MHz in the 400th RF cycle, and 27.12 MHz in the 800th RF cycle at times $t = 1/4T$, $2/4T$, $3/4T$, and $4/4T$ are plotted in Fig. 6. For the four driving frequencies, at the time $t = 1/4T$, in the region $0 \le x \le d/2$, the electron heating is negative; in the region $d/2 \le x \le d$, the electron heating is positive and there

is a peak of the electron heating. This means that at the time $t = 1/4T$, in the region $0 \le x \le d/2$, the electron heating cools the electrons, and in the region $d/2 \le x \le d$, the electron heating heats the electrons. For the four driving frequencies, at time $t = 2/4T$, in the region $0 \le x \le d/2$, the electron heating is positive and there is a higher peak of the electron heating; in the region $d/2 \le x \le d$, the electron heating is negative and there is a higher negative peak of the electron heating. This means that at the time $t = 2/4T$, in the region $0 \le x \le d/2$, the electron heating heats the electrons, and in the region $d/2 \le x \le d$, the electron heating cools the electrons. For the four driving frequencies, at time $t = 3/4T$, the electron heating is just the mirror-imaged one at time $t = 1/4T$. For the four driving frequencies, at time $t = 4/4T$, the electron heating is almost the same as the one at time $t = 2/4T$. As the driving frequency increases, the electron heating increases negatively or positively.

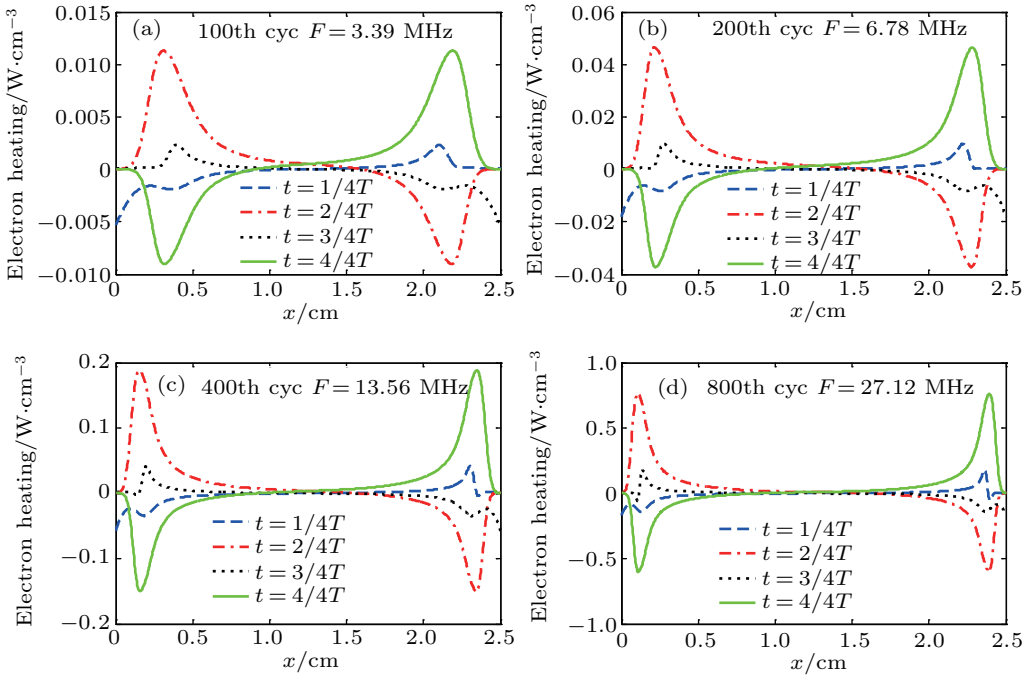


Fig. 6. (color online) Spatial distributions of electron heating with driving frequencies of (a) 3.39 MHz in the 100th cycle, (b) 6.78 MHz in the 200th cycle, (c) 13.56 MHz in the 400th cycle, and (d) 27.12 MHz in the 800th cycle, at times of $1/4T$, $2/4T$, $3/4T$, and $4/4T$.

4. Conclusions

A 1D fluid model for a capacitive RF argon discharge at low pressure is established to study the effect of the driving frequency on electron heating. The numerical results of the evolutions of the discharge process are obtained. The results show that the discharge process has three stages: the growing rapidly stage, the growing slowly stage and the steady stage. In the steady stage, the maximal electron density increases as the driving frequency increases. Also, the results of the cycle-averaged electric field, electron temperature, electron density and electric potential for the driving frequencies of 3.39, 6.78, 13.56, and 27.12 MHz are compared. The results show that the discharge region has three parts: the powered electrode sheath region, the bulk plasma region, and the grounded electrode sheath region. The width of the sheath regions decreases as driving frequency increases. At 18 μs, the cycle-averaged electron pressure cooling, electron ohmic heating, electron heating and electron energy loss for the driving frequencies of 3.39, 6.78, 13.56, and 27.12 MHz are compared. The results indicate that the electron pressure cooling cools the electrons and the electron ohmic heating heats the electrons, the electron heating heats the electrons in the discharge region except in the regions near the electrodes. The heating (cooling) effect increases as the driving frequency increases. Furthermore, the results of the electron pressure cooling, electron ohmic heating and electron heating, for the driving frequencies of 3.39 MHz in the 100th cycle, 6.78 MHz in the 200th cycle,13.56 MHz in the 400th cycle, and 27.12 MHz in the 800th cycle, at four times in one RF-cycle: $1/4T$, $2/4T$, $3/4T$, and $4/4T$ are compared. It is found that the electron heating has the heating and cooling effect on the electrons alternatively in one cycle.

References

[1] Makabe T, Nakano N and Yamaguchi Y 1992 *Phys. Rev. A* **45** 2531
[2] Richards D, Thompson B E and Sawin H H 1987 *Appl. Phys. Lett.* **50** 494
[3] Conti S, Porshnev P I, A Fridman, Kennedy L A, Grace J M, Sieber K D, Freeman D R and Robinson K S 2001 *Experimental Thermal and Fluid Science* **24** 91
[4] Vahedi V, Birdsall C K, Lieberman M A, DiPeso G and Rognlien T D 1993 *Plasma Sources Sci. Technol.* **2** 278
[5] Vahedi V, DiPeso G, Birdsall C K, Lieberman M A and Rognlien T D 1993 *Plasma Sources Sci. Technol.* **2** 272

[6] Kushner M J 1983 *J. Appl. Phys.* **54** 4965
[7] Meyyappan M and Govindan T R 1993 *J. Appl. Phys.* **74** 2259
[8] Lymberopoulos D P and Economou D J 1993 *J. Appl. Phys.* **73** 3679
[9] Lymberopoulos D P and Economou D J 1995 *J. Phys. D: Appl. Phys.* **28** 737
[10] Berezhnoi S V, Kaganovich I D and Tsendin L D 1998 *Plasma Physics Reports* **24** 563
[11] Park S K and Economou D J 1990 *J. Appl. Phys.* **68** 3915
[12] Rakhimova T V, Braginsky O V, Ivanov V V, Kim T K, Kong J T, Kovalev A S, Lopaev D V, Mankelevich Y A, Proshina O V and Vasilieva A N 2006 *IEEE Trans. Plasma Sci.* **34** 877
[13] Donkó Z, Schulze J, Czarnetzki U, Derzsi A, Hartmann P, Korolov I and Schüngel E 2012 *Plasma Physics and Controlled Fusion* **54** 124003
[14] Surendra M and Graves D B 1991 *Appl. Phys. Lett.* **59** 2093
[15] Nakano N and Makabe T 1995 *J. Phys. D: Appl. Phys.* **28** 39
[16] Segawa S, Kurihara M, Nakano N and Makabe T 1999 *Jpn. J. Appl. Phys.* **38** 4422
[17] Colgan M J, Meyyappan M and Murnick D E 1994 *Plasma Sources Sci. Technol.* **3** 189
[18] Vahedi V, Birdsall C K, Lieberman M A, DiPeso G and Rognlien T D 1993 *Phys. of Fluids B* **5** 2729
[19] Georgieva V, Bogaerts A and Gijbels R 2003 *J. Appl. Phys.* **94** 3756
[20] Lee J K, Babaeva N Y, Kim H C, Manuilenko O V and Shon J W 2004 *IEEE Trans. Plasma Sci.* **32** 53
[21] Surendra M and D B Graves 1991 *IEEE Trans. Plasma Sci.* **19** 157
[22] Kawamura E, Lieberman M A and Lichtenberg A J 2006 *Phys. Plasmas* **13** 053506
[23] Kitajima T, Takeo Y, Nakano N and Makabe T 1998 *J. Appl. Phys.* **84** 5936
[24] Boeuf J P 1987 *Phys. Rev. A* **36** 2792
[25] Zhu X M, Chen W C, Zhang S, Guo Z G, Hu D W and Pu Y K 2007 *J. Phys. D: Appl. Phys.* **40** 7023
[26] Graves D B 1987 *J. Appl. Phys.* **62** 94
[27] Surendra M, Graves D B and Morey I J 1990 *Appl. Phys. Lett.* **56** 1024
[28] Lieberman M A and Godyak V A 1998 *IEEE Trans. Plasma Sci.* **26** 986
[29] Chen G and Raja L L 2004 *J. Appl. Phys.* **96** 6081
[30] Abdel-Fattah E and Sugai H 2003 *Appl. Phys. Lett.* **83** 1535
[31] Nitschke T E and Graves D B 1994 *J. Appl. Phys.* **76** 5660
[32] Turner M M 1995 *Phys. Rev. Lett.* **75** 1315
[33] Graves D B and Jensen K F 1986 *IEEE Trans. Plasma Sci.* **PS-14** 91
[34] Liu Q, Liu Y, Samir T and Ma Z 2014 *Phys. Plasmas* **21** 083511
[35] Lafleur T, Chabert P and Booth J P 2014 *Plasma Sources Sci. Technol.* **23** 035010